# MODELING AND SIMULATION OF WIDEBAND RADIO CHANNEL CHARACTERIZATION FOR AN URBAN LINE-OF-SIGHT MICROCELL

Hassan M. El-Sallabi[1] and Pertti Vainikainen
Radio Laboratory, Institute of Radio Communications (IRC)
Helsinki University of Technology
P. O. Box 3000, FIN-02015 HUT, Finland
Tel: +358 9 451 22 55 Fax: +358 9 451 2152
E-mail: [1]hel@radio.hut.fi

**Abstract**

**This paper presents a proposed model in an explicit form and its simulation results for characterizing wideband line-of-sight (LOS) radio channel in an urban microcellular environment. The model is fast to compute, easy to implement, and only those rays that reach the receiver locations are calculated. Effect of street-grid, with any number of crossing streets of different widths, on the propagation characteristics can be studied. The model provides details of possible radio paths that join the basestation with the mobile terminal at any point in the main street. The characterization of the channel is presented in three domains. They are: frequency, temporal and angular domains. The model can be used to study several microcellular communication problems.**

## I. Introduction

The recent trend to increase the capacity of cellular systems has led to the adoption of the concept of microcells [1-3]. The antenna placement below rooftops results in the propagation mechanism that is dominated by multiple reflections [2,3] which is strongly affected by street structure and wall reflectivity. The detailed characterization of the radio channel propagation is a major requirement for successful design of wireless communication system. This paper presents modeling and simulation results for characterizing wideband propagation channel. The model is given in an explicit form. Thus, it is fast to compute, easy to implement, and only those rays that reach the receiver locations are calculated. This work models LOS propagation in urban streets which are usually crossed by some number of side-streets that vary in widths. This model is proposed in terms of multiple wall-wall reflections rays approaching the observer along a direct and ground reflected rays. The number of wall-wall reflected rays is spatial-variant. Models with fixed number of rays, (i.e., six and ten rays) are proposed in [4] and [5], respectively. Corner diffracted rays are ignored as proposed in [6][7]. Curved corner reflection is not considered, it is presented in [8]. Over rooftop rays are neglected.

## II. Channel transfer function formulation

Let $H(f)$ be the transfer function of a spatial-variant multiray channel, where $f$ is the frequency. Specifically, $|H(f)|^2 = P_r/P_t$, where $P_t$ and $P_r$ are the transmitted and received powers, respectively. The urban city street under study is shown in Fig. 1. The received power is given by

$$P_r = P_t \left| G_d H_d + G_g H_g + \sum_{i=1}^{M} G_i H_i \right|^2 \qquad (1)$$

where $H_d = \lambda e^{-jkr_d} / (4\pi r_d)$ and $H_g = R_g \lambda e^{-jkr_g} / (4\pi r_g)$

$H_i(f) = \Gamma_i \lambda e^{-jkr_i} / (4\pi r_i)$ are the direct, ground reflected, and $i^{th}$ wall-wall reflected rays transfer functions, respectively, $\lambda$ is the wavelength, $k$ is the wave number, $R_g$ is well known Fresnel reflection coefficient [3] for ground reflected ray, $G_d$, $G_g$, and $G_i$ are the products of BS and MS antenna field patterns corresponding to the path of direct, ground reflected, and the $i^{th}$ wall reflected rays with the proper transmission and arrival angles. The $r_d$, $r_g$ and $r_i$ are the path lengths of the direct, ground reflected, and $i^{th}$ wall-wall reflected rays, they are given by

$$r_{d,g} = \left[ d^2 + (h_B \mp h_M)^2 \right]^{1/2} \qquad (2)$$

where "-" and "+" correspond to $r_d$ and $r_g$, respectively, $h_B$ and $h_M$ are the basestation and mobile antenna heights, respectively, $d = \sqrt{x^2 + (w - y_0 - y_1)^2}$, $w$ is street width, $x$, $y_0$, and $y_1$ are shown in Fig. 1. Since calculation of both phase and amplitude of $H(f)$ requires the path lengths of the rays, an explicit form is derived by

using image theory. The ray path lengths for even ($r_{ie}$) and odd ($r_{io}$) number of reflections are written as

$$r_{ie} = \sqrt{x^2 + \left((m \pm 1)w \mp y_o \mp y_1\right)^2 + \Delta h^2} \quad (3)$$

$$r_{io} = \sqrt{x^2 + \left(mw \pm y_o \mp y_1\right)^2 + \Delta h^2} \quad (4)$$

where $\Delta h = h_B - h_M$. The selection of "-" and "+" signs is done by choosing upper (lower) signs together. Let $\mathcal{M}$ be the selected maximum reflection order. For each number of wall-wall reflections $m$=1,2,..,$\mathcal{M}$, there are two different rays that differ at least in angle of arrival. Thus, there is a maximum $M = 2\mathcal{M}$ different wall-wall reflection rays. The angular information which is needed for the potential use of adaptive array antennas at the basestation is obtained as follows: The azimuth ($\phi$), elevation ($\theta$) angles can be calculated from

$$\phi_{ie} = \mp \arctan\left(\left((m \pm 1)w \mp y_o \mp y_1\right)/x\right) \quad (5)$$

$$\theta_{ie} = \pi - \arctan\left(\sqrt{x^2 + \left((m \pm 1)w \mp y_o \mp y_1\right)^2}/\Delta h\right) \quad (6)$$

for even number of wall-wall reflections and

$$\phi_{io} = \pm \arctan\left(\left(mw \pm y_o \mp y_1\right)/x\right) \quad (7)$$

$$\theta_{io} = \pi - \arctan\left(\sqrt{x^2 + \left(mw \pm y_o \mp y_1\right)^2}/\Delta h\right) \quad (8)$$

for odd number of wall-wall reflections. The zero-degree for elevation direction is the vertical direction. The zero-degree for azimuthal direction is shown on Fig. 1. The positive angle is counter-clock wise direction. The reflection coefficient $\Gamma_i$ for $H_i(f)$ is obtained by Fresnel reflection coefficient. The coefficients $R_g$ and $\Gamma_i$ are functions of incidence angles which can be written as

$$\alpha_g = \arctan\left(\left(h_B + h_M\right)/d\right) \quad (9)$$

for ground reflected ray and

$$\alpha_{ie} = \arctan\left(\left((m \pm 1)w \mp y_o \mp y_1\right)/\sqrt{x^2 + \Delta h^2}\right) \quad (10)$$

for rays with even number of wall-wall reflections and

$$\alpha_{io} = \arctan\left(\left(mw \pm y_o \mp y_1\right)/\sqrt{x^2 + \Delta h^2}\right) \quad (11)$$

for rays with odd number of wall-wall reflections. When street grid exists between basestation and mobile terminal, all wall-wall reflected rays do not reach every receiver location. The rays that reach the receiver position are determined by the reflection angles as

$$\alpha_i \notin \left\{\left\{\alpha_i : \alpha_{1W62} < \alpha_i < \alpha_{1W61}\right\} \cup \left\{\alpha_i : \alpha_{2W62} < \alpha_i < \alpha_{2W61}\right\} \cup \left\{\alpha_i : \alpha_{3W62} < \alpha_i < \alpha_{3W61}\right\}\right\} \quad (12)$$

where

$$\alpha_{pWSg} = \arctan\left(\frac{(m - (2 - S))w - (-1)^S y_1}{\sqrt{x_{pWGg}^2 + \Delta h^2}}\right) \quad (13)$$

where $p$=1,2, and 3 (i.e. crossing streets 1, 2, and 3), $g$=1,2, $S$=1(2) is for the two side walls, it is related to lower(upper) "+" and "-" signs of (3) and (4), and $G = S^{(S-1)}\left(S^{(S-2)} + [2 - S]\right)$ for odd (even) values of $m$. The parameter $x_{pWGg}$ is shown on Fig. 1.

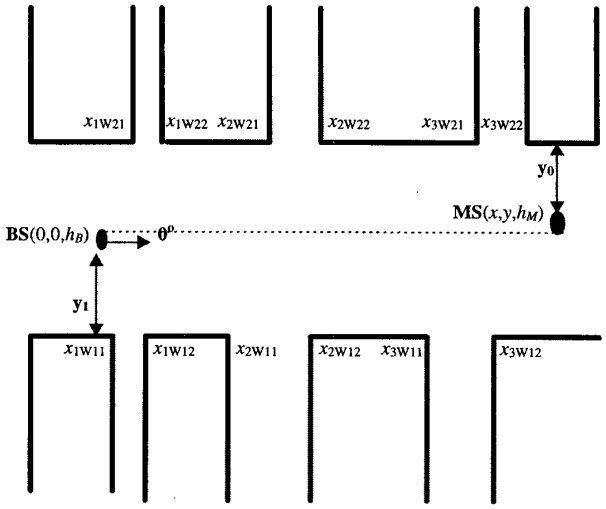


*Fig. 1. Urban LOS microcellular environment with MS route along the main street is shown with corner positions.*

## III. Results and discussion

The computation results presented here are for characterizing propagation in the city street shown in Fig. 1. Building database are given in Table 1. Base and mobile antenna heights of 13.3m and 1.6m, respectively, are chosen to emulate a typical microcellular scenario [9]. Isotropic antennas for both the BS and MS are assumed. Selection of $\mathcal{M}$ =10 is used in later computation. The values of $w$=20m, $y_0$=18m, and $y_1$=1.5m $x$ =10 to 320m in steps of one meter are selected. Carrier frequency is $f_o$=2.154 *GHz*. In order to have detailed characterization of the channel, it is characterized in frequency, temporal and angular domains.

Table 1:Building database used in model simulation, units are in meter.

| $x_{1W21}$ | $x_{1W11}$ | $x_{1W22}$ | $x_{1W12}$ | $x_{2W21}$ | $x_{2W11}$ | $x_{2W22}$ | $x_{2W12}$ | $x_{3W21}$ | $x_{3W11}$ | $x_{3W22}$ | $x_{3W12}$ |
|---|---|---|---|---|---|---|---|---|---|---|---|
| 25 | 25 | 40 | 40 | 120 | 130 | 149 | 165 | 245 | 250 | 163 | 285 |

a) **Number of paths and reflection order**

Fig. 2a shows simulation results for the number of paths that join the transmitter and receiver at points on the traveling route of MS in the main street. Twenty wall-wall reflected paths (i.e., $M=2\mathcal{M}$) connect the BS and MS just before the first street junction. The number of paths varies from location to other when the street junctions are included in the traveling route. The number of paths that connect transmitter and receiver depend on both the BS and MS locations. In Fig. 2a, there are receiver locations (i.e., $x$=64 to 75m) where no wall-wall reflected paths joining the BS and MS exist. Only direct and ground reflected path exist in these locations. Fig. 2b depicts the relative occurrence frequency of paths of each reflection order. About 90% of joining paths have up to the 8th reflection order. As the reflection order increases the probability of its occurrence decreases.

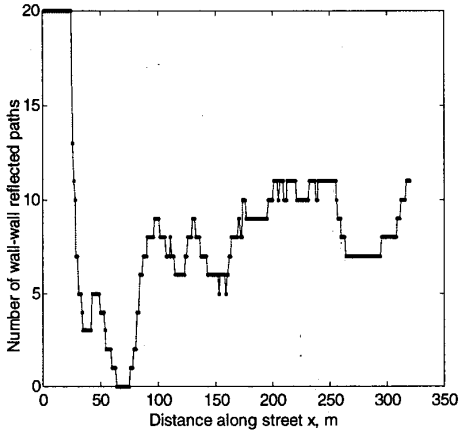


(a)

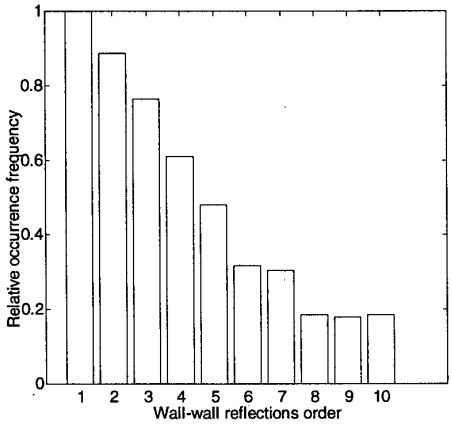


(b)

*Fig. 2. (a) Number of wall-wall reflected paths join BS and MS along main street. (b) Relative frequency of rays of specific reflection order.*

b) **Frequency domain characterization**

The channel transfer function is described by its magnitude and phase. The wideband channel transfer function is simulated by discrete frequency computation across the desired RF band [8]. The magnitude of the channel transfer function for MS route is shown in Fig. 3a for the frequency range $f_o \pm 50MHz$. It gives the narrrowband path loss, it also provides information about the frequency selective fading pattern. The phase of the channel transfer function is presented in terms of group delay. The group delay results are shown in Fig. 3b. Spikes occur nearly at the same frequency as the magnitude fades. It is seen that depth of the frequency selective fading depth and group delay spikes change with the distance between mobile station and side walls. Frequency selective fading depth and group delay spikes also vary with the wall electrical properties. The results shown in Fig.3 are for $\varepsilon_r$=15 and $\sigma$ = 0.005 S/m.

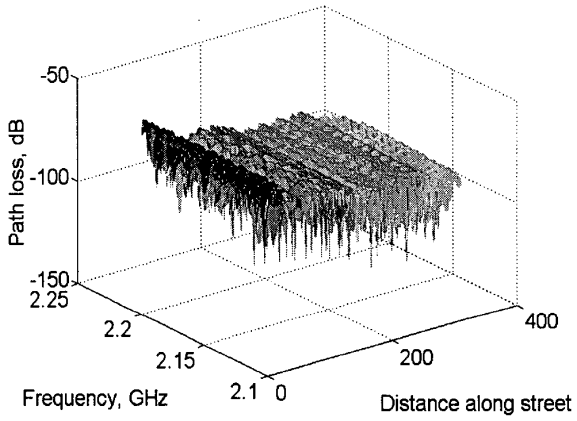


(a)

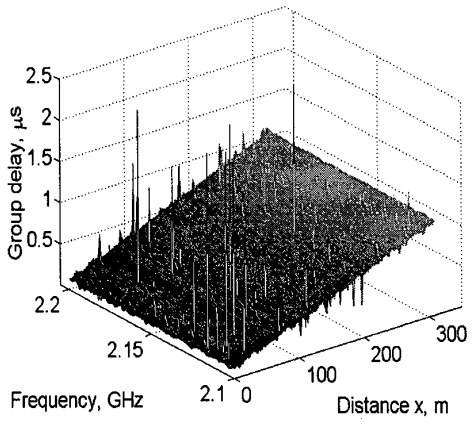


(b)

*Fig. 3. (a) Magnitude of spatial variant channel transfer function, (b) Group delay.*

c) **Time domain characteristics**

The complex delay profiles at each position of the MS can be obtained from the developed model. This allows us to investigate the space-variant characteristics of the delay profile. Since the measurements systems are bandlimited, the model can simulate bandlimited channels. The simulation results of spatial-variant bandlimited time domain path loss is shown in Fig. 4a. The root mean square (RMS) delay spread (RDS) can also be calculated. The importance of the delay spread is well known, as it describes the dispersion in time domain and thereby inter-symbol-interference. Fig. 4b depicts the RDS obtained from impulse response of the channel. It is seen that the RDS has higher values for locations when MS is closer to the BS. The RDS has minimum values at locations where no wall-wall reflected paths join the BS and MS (i.e., $x$=64 to75m, see Fig. 2a).

d) **Angular domain characteristics**

Radio waves arrive at the receiver from a number of azimuthal directions. Fig. 5a depicts the space-variant power azimuth-angle profile relative to the maximum strength of power angular profile along MS route. It is seen that arrival angle range reduces as the MS gets further away. The RMS angular spread (RAS) which is the angular domain dispersion parameter, is defined here as the square root of the second central moment of the power angular profile. Fig. 5b shows the RAS for each MS position along the traveling route. At MS locations $x$=64 to 75m where there is no wall-wall reflection rays (see Fig. 2a) the RAS is zero. Larger variation of the RMS angular spread can be seen for locations before the street grid exist between BS and MS. The variation of the RAS reduces as the MS travels further a way from BS. Fig. 6 depicts scatter plot of the RAS versus RDS. It is clear that there is correlation between the two parameters.

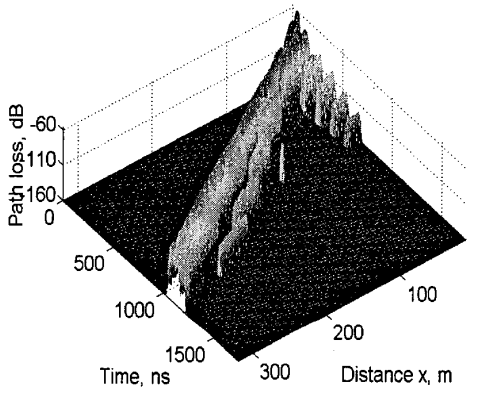


(a)

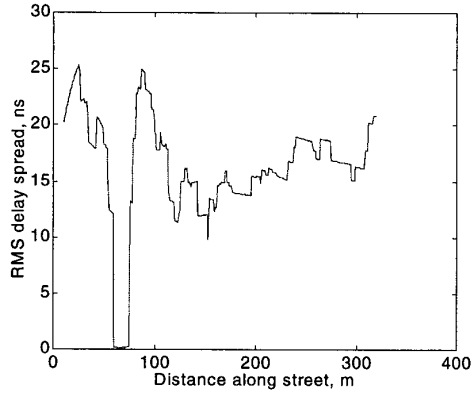


(b)

*Fig. 4. (a) Space-variant time domain path loss, (b) The RMS delay spread.*

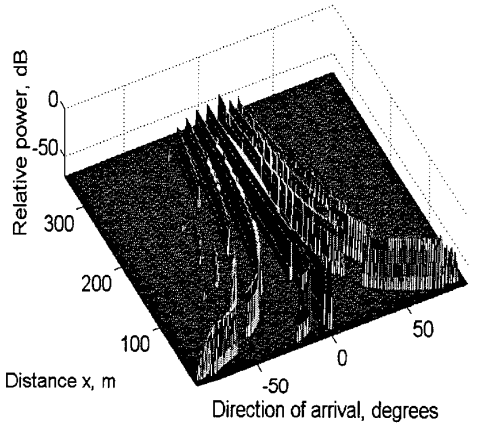


(a)

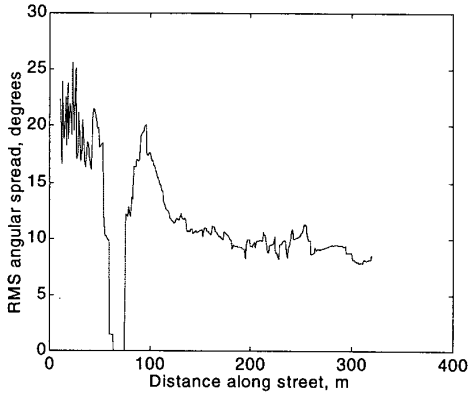


(b)

*Fig. 5. (a) Space-variant relative power azimuth angle profile, (b) The RMS angular spread.*

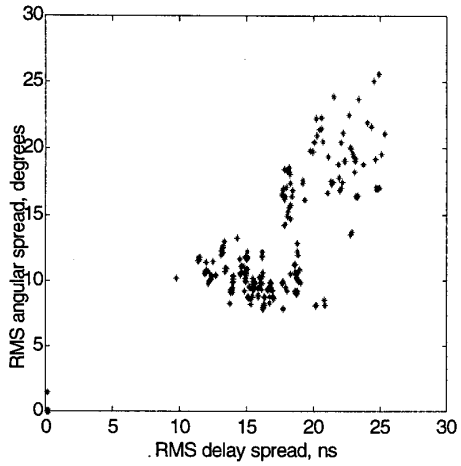


*Fig. 6. The RMS angular and delay spread scatter.*

## IV. Conclusion

This work presents modeling and simulation results for wideband LOS propagation in microcell. The model is presented in an explicit form. The developed model can be made for urban LOS with street grid of any number of crossing streets and with different widths. Effect of street-grid on the propagation characteristics can be studied. The simulation results of channel characterization are presented here in three domains which are frequency, time and angular domains. The model provides details of possible radio paths that join the basestation with the mobile terminal at any point in the main street. It is found that the angular domain spread reduces as the MS travels further away from the BS. The propagation characteristics changes with different wall properties. The model can be used to study several microcellular mobile communications problems.

## References

[1] H. L. Bertoni, W. Honcharenko, L. R. Maciel, and H. Xia, "UHF propagation for wireless personal communications," *Proc. IEEE*, vol. 82, pp. 1333 - 1359, Sep. 1994.

[2] U. Dersch and E. Zollinger, "Propagation mechanisms in microcell and indoor environment," *IEEE Trans. Antennas and Propagat.*, vol. 43 pp. 1058-1066, Nov. 1994.

[3] K. Rizk, J.-F. Wagen, and F. Gardiol, "Two-dimensional ray-tracing modeling for propagation in microcellular environments," *IEEE Trans. Veh. Technol.*, vol. 46, pp. 508-518, Feb. 1997.

[4] A. J. Rustako, N. Amitay, G. J. Owen, and R. S. Roman, "Radio propagation at microwave frequencies for line-of-sight microcellular mobile and personal communications," *IEEE Trans. Veh. Technol.*, vol. 40 pp. 203-210, Feb. 1991.

[5] N. Amitay "Modeling and computer simulation of wave propagation in lineal line-of-sight microcells," *IEEE Trans. Veh. Technol.*, vol. 41 pp. 337-342, Nov. 1992.

[6] R. Mazar, A. Bronshtein, and I.-Tai, " Theoretical analysis of UHF propagation in a city street modeled as a random multislit waveguide," *IEEE Trans. Antennas and Propagat.*, vol. 46 pp. 864-871, Jun. 1998.

[7] S. Y. Tan and H. S. Tan, "A microcellular communications propagation model based on the uniform theory of diffraction and multiple image theory," *IEEE Trans. Antennas and Propagat.*, vol. 44, pp.1317-1326, Oct. 1996.

[8] H. M. El-Sallabi, W. Zhang, K. Kalliola, and P. Vainikainen, "Full 360° azimuth angle wideband propagation modeling for an urban Line-of-sight microcellular environment," Proc. of *IEEE International Communication Conf., (ICC'99),* pp. 1608-1612, June-1999, Vancouver, Canada.

[9] Feuerstein, M. J., K. L. Blackard, T. S. Rappaport, S. Y. Seidel, and H. H. Xia, "Path loss, delay spread, and outage models as functions of antenna of height for microcellular system design," *IEEE Trans. Veh. Technol.*, Vol. 43 pp. 487-498, Aug. 1994.